

Estimating Shapley Effects in Big-Data Emulation and Regression Settings using Bayesian Additive Regression Trees

Akira Horiguchi*

Department of Statistical Science, Duke University

and

Matthew T. Pratola

Department of Statistics, The Ohio State University

Abstract

Shapley effects are a particularly interpretable approach to assessing how a function depends on its various inputs. The existing literature contains various estimators for this class of sensitivity indices in the context of nonparametric regression where the function is observed with noise, but there does not seem to be an estimator that is computationally tractable for input dimensions in the hundreds scale. This article provides such an estimator that is computationally tractable on this scale. The estimator uses a metamodel-based approach by first fitting a Bayesian Additive Regression Trees model which is then used to compute Shapley-effect estimates. This article also establishes a theoretical guarantee of posterior consistency on a large function class for this Shapley-effect estimator. Finally, this paper explores the performance of these Shapley-effect estimators on four different test functions for various input dimensions, including $p = 500$.

Keywords: Nonparametric, functional ANOVA, global sensitivity analysis, variable importance, surrogate model

*AH would like to acknowledge Miheer Dewaskar for fruitful discussions. The work of MTP was supported in part by the National Science Foundation under Agreements DMS-1916231, OAC-2004601, and in part by the King Abdullah University of Science and Technology (KAUST) Office of Sponsored Research (OSR) under Award No. OSR-2018-CRG7-3800.3.

1 Introduction

An important task in global sensitivity analysis is to measure how a function depends on its various inputs. A popular measure of variable importance is the class of Sobol' indices (Sobol', 1990), which decomposes the variance of outputs from a function into terms due to main effects for each input and interaction effects between the various inputs. To quantify the impact of any particular input dimension, either the *main-effect Sobol' index* or the *total-effect Sobol' index* can be used; the latter includes all interactions between the given input and any other input whereas the former excludes any such interaction. Straightforward interpretation of Sobol' indices requires an orthogonal distribution on the inputs (Song et al., 2016). *Shapley effects* (Shapley, 1952; Song et al., 2016) form another class of variance-based global sensitivity indices that was first introduced in the context of game theory but has only recently been gaining traction in the statistics literature (Owen, 2014). Although the additional computation required to compute Shapley effects might render them unnecessary if the inputs are known to be independent, Shapley effects remain interpretable even if the inputs are correlated (Song et al., 2016) and hence are the more reasonable option in such a case.

A function's Sobol' indices and Shapley values can, on occasion, be computed exactly, particularly when a closed-form expression of the function is known and the required expectations can be evaluated easily. But more often than not, computing these expectations requires some sort of integral approximation. Monte Carlo integration is a simple option and is used to estimate Shapley effects by e.g. Song et al. (2016); Benoumechiara and Elie-Dit-Cosaque (2019); Broto et al. (2020); Plischke et al. (2021); Goda (2021). Figure 1 shows various Shapley-effect estimators applied to n observations generated from the Sobol' g -function (defined in the figure caption) evaluated on i.i.d. inputs drawn uniformly from the hypercube $[0, 1]^5$. When the function values are observed without noise, these methods track the g -function's true Shapley-effects very well. But when independent and identically distributed (i.i.d.) Gaussian noise with mean zero and moderate variance (defined in the figure caption) is added, these methods struggle to capture the true values even when the number of observations increases dramatically to compensate for the observation noise.

Another option is to first fit a metamodel which can then be used to compute estimates of Sobol' indices and Shapley effects as a post-processing step. This approach is also useful when a function can only be sparsely evaluated, necessitating the use of a metamodel. Popular metamodels for this purpose include the Gaussian Process (GP), Bayesian multivariate adaptive regression splines (BMARS) (Denison et al., 1998), generalized polynomial chaos expansions (PCE) (Sudret, 2008), treed GPs Gramacy and Taddy (2010), dynamic trees (Gramacy et al., 2013), Gaussian radial basis function (Wu et al., 2016), artificial neural networks (Li et al., 2016), and deep GPs (Radaideh and Kozlowski, 2020). This paper makes its contributions using Bayesian Additive Regression Trees (BART) (Chipman et al., 2010) which is an increasingly popular tool for complex regression problems and as emulators of expensive computer simulations (Chipman et al., 2012; Gramacy and Haaland, 2016; Horiguchi et al., 2022). BART is a nonparametric sum-of-trees model embedded in a Bayesian inferential framework. Unlike many other metamodels, BART can easily incorporate categorical inputs, avoids strong parametric assumptions, and is relatively quick to fit even on a large number of observations. BART even has been shown to be resilient to the inclusion of inert inputs, particularly when the BART prior incorporates either the

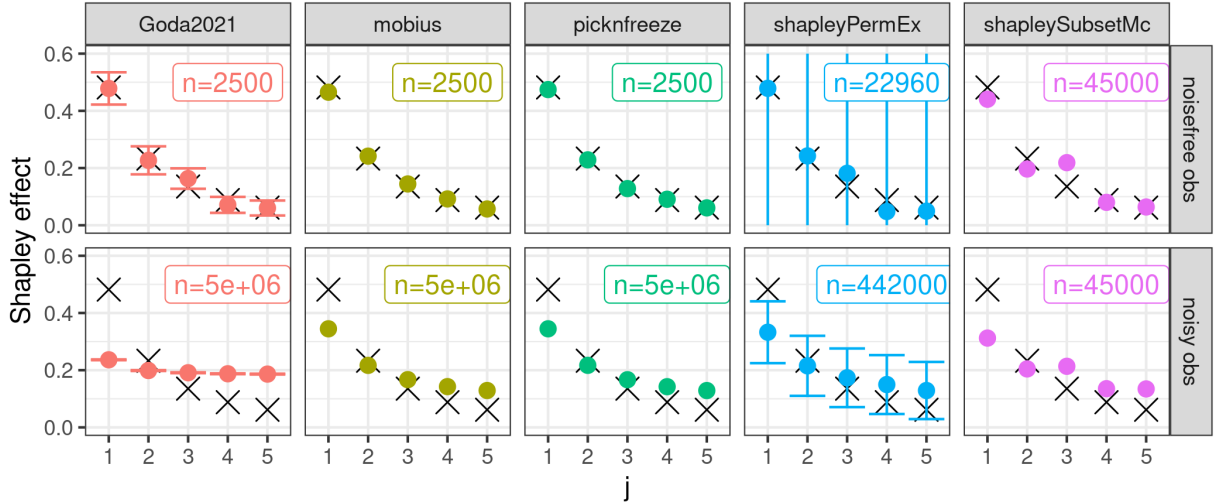


Figure 1: Shapley-effect estimates of various existing methods trained on data drawn from the Sobol' g -function $f(\mathbf{x}) = \prod_{k=1}^5 \frac{|4x_k - 2| + (k-1)/2}{1 + (k-1)/2}$. Crosses represent the true Shapley-effect values. Function values are evaluated at n i.i.d. inputs drawn uniformly from the hypercube $[0, 1]^5$. In the top row, function values are observed without noise. In the bottom row, the observations are function values plus i.i.d. Gaussian noise with mean zero and variance 0.25×3.076 , where 3.076 is the variance of the g -function under a uniform distribution on $[0, 1]^5$. Each column represents an estimation method: “Goda2021” is from Goda (2021); “mobius” and “picknfreeze” are from Plischke et al. (2021); “shapleyPermEx” and “shapleySubsetMc” are from Iooss et al. (2023). Error bars represent approximate or exact 95% confidence intervals as implemented by the method.

sparsity-inducing Dirichlet prior of Linero (2018) or the spike-and-tree prior of van der Pas and Ročková (2017); Liu et al. (2021). Furthermore, the Bayesian framework provides natural uncertainty quantification for both predictions and sensitivity-index estimates.

Some metamodels struggle more than others with the two computational stages in the above approach, namely fitting the metamodel, then using the fitted metamodel to estimate the sensitivity indices. Regarding the former stage, many of these metamodel-based approaches struggle to fit if the number of inputs p and function evaluations n is not small. A GP has $O(n^3)$ computation time and struggles to fit for even $p = 10$. PCE has been fit for $p = 25$, but it has been noted that PCE struggles to fit for larger p (Sudret, 2008; Crestaux et al., 2009). BMARS works for $p = 200$ for Sobol' indices (Francom et al., 2018). Section 5.2 of this paper provides an example where BART fits to a $p = 500$ scenario with $d = 250$ active variables. Regarding the latter stage, BART (Horiguchi et al., 2021), BMARS (Francom et al., 2018), and PCE (Sudret, 2008) have closed form expressions for Sobol' indices (and thus for Shapley effects) that can be computed exactly once the metamodel is fit. Such expressions also exist for GPs with polynomial mean and either a separable Gaussian, Bohman, or cubic correlation function (Oakley and O'Hagan, 2004; Chen et al., 2005, 2006; Marrel et al., 2009; Moon, 2010; Svenson et al., 2014; Santner et al., 2018). Table 1 summarizes these metamodel properties.

To the best of our knowledge, this article is the first to provide an estimator of a function's *Shapley effects* that is computationally tractable for a relatively large number of

		Consistency established?	Adapt to discontinuities in regression function?	UQ	Tractable to fit model for $p = 250$?	Analytical expression for Shapley effects or Sobol' indices?	Available code to estimate Shapley effects?
	BART	yes (Jeong and Rockova, 2023)	yes (Jeong and Rockova, 2023)	Bayesian	yes (Section 5)	yes (Horiguchi et al., 2021)	this paper (Pratola, 2023)
	GP	yes	yes (Mohammadi et al., 2019)	Bayesian	no	yes for some covariance kernels	sensitivity R package (Iooss and Prieur, 2019)
	PCE	no	no	bootstrap	no	yes (Sudret, 2008)	no
BMARS		no	no	Bayesian	yes (Francom et al., 2018)	yes (Francom et al., 2018)	no

Table 1: Properties of various metamodels under nonparametric regression.

inputs and function evaluations, as well as provide theoretical guarantees of consistency in the context of nonparametric regression where the function is observed with noise. The computation of our estimators relies on a particular feature of BART, namely that the sum-of-trees model assumption implies every realization of a BART random function is piecewise constant. Horiguchi et al. (2021) leverages this feature to establish closed-form expressions for Sobol' index estimates computed using a fitted BART model (such estimates will be denoted as “BART-based Sobol' indices” for the rest of this article) that are easy to compute after the BART model is fit. Section 2 will show these closed-form expressions can be used to compute BART-based Shapley effects, but because the number of expressions to compute increases dramatically, Section 4 discusses computationally friendly approximations. On the other hand, our contraction-rate results rely heavily on recent BART theory from Jeong and Rockova (2023), who introduce the large class of sparse piecewise heterogeneous anisotropic Hölder functions and show that over this function class, the contraction rate for Bayesian forests is optimal up to a logarithmic factor.

This article is organized as follows. Section 2 reviews BART, piecewise heterogeneous anisotropic functions, Sobol' indices, and Shapley effects. Section 3 provides posterior contraction for BART-based Sobol' indices and Shapley effects. Section 4 discusses computation of BART-based Shapley effects. Section 5 showcases their performance on numerical examples, including a data from the En-Roads climate simulator (analogous discussion for BART-based Sobol' indices can be found in Horiguchi et al. (2021)). Section 6 provides discussion on future work. Proofs of results are included as Supplementary Material.

1.1 Notation

For any positive integer m , denote $[m] := \{1, \dots, m\}$. We also distinguish between any subset \subseteq and a proper subset \subset . Let $L^2 \equiv L^2([0, 1]^p)$ denote the space of real-valued, square-integrable functions on the unit hypercube $[0, 1]^p$. Finally, let \mathbb{E} and \mathbb{V} respectively denote the expectation and variance operator.

2 Review

Mirroring Jeong and Rockova (2023), this article considers regression settings with either a fixed or random design. The regression model with *fixed* design is

$$Y_i = f_0(\mathbf{x}_i) + \varepsilon_i, \quad \varepsilon_i \sim N(0, \sigma_0^2), \quad i = 1, \dots, n, \quad (1)$$

where $\sigma_0^2 < \infty$ and each covariate $\mathbf{x}_i \in [0, 1]^p$ is fixed. A fixed design would be assumed if, for example, the trees in BART are allowed to split only on observed covariate values (which was a specification used in the seminal BART paper (Chipman et al., 2010)) or on dyadic midpoints of the domain. The regression model with *random* design is

$$Y_i = f_0(\mathbf{X}_i) + \varepsilon_i, \quad \mathbf{X}_i \sim \pi, \quad \varepsilon_i \sim N(0, \sigma_0^2), \quad i = 1, \dots, n, \quad (2)$$

where $\sigma_0^2 < \infty$, each $\mathbf{X}_i \in [0, 1]^p$ is a p -dimensional random covariate, and π is a probability measure such that $\text{supp}(\pi) \subseteq [0, 1]^p$. A random design would be assumed for estimation problems such as density estimation or regression/classification with random design. Our results in Section 3 deal separately with fixed or random designs.

2.1 BART

In a regression setting in the form of either (1) and (2), a BART model approximates the unknown function f_0 by a sum of T regression trees:

$$f_0(\cdot) \approx \sum_{t=1}^T g(\cdot; \Theta_t), \quad (3)$$

where each regression-tree function $g(\cdot; \Theta_t) : [0, 1]^p \rightarrow \mathbb{R}$ is piecewise constant over the input space. Each parameter set Θ_t determines a partition of the input space $[0, 1]^p$ into boxes (i.e. hyperrectangles) and the fitted response values assigned to each partition piece. The partition is induced by recursively applying binary splitting rules; Figure 2 shows an illustrative example. To regularize the model fit, the BART prior over the parameters $\{\Theta_t\}_{t=1}^T$ keeps the individual tree effects small, which causes each function $g(\cdot; \Theta_t)$ to contribute a small portion to the total approximation of f_0 . The expected response $\mathbb{E}[Y(\mathbf{x}) | \{\Theta_t\}_{t=1}^T]$ at a given input \mathbf{x} is then the sum of each contribution $g(\mathbf{x}; \Theta_t)$.

Though the right hand side of (3) is piecewise constant, Jeong and Rockova (2023) shows that under certain conditions, BART can approximate the unknown function f_0 (which itself need not be piecewise constant) arbitrarily closely with attractive posterior contraction rates. After reviewing the concept of contraction rates, we state for convenience the conditions made in the theorems of Jeong and Rockova (2023) that our contraction-rate results rely on. Because these conditions are not the focus of this paper, we leave discussion of the context behind these conditions to Jeong and Rockova (2023).

2.1.1 Piecewise heterogeneous anisotropic functions

Next we introduce the conditions of the theorems of Jeong and Rockova (2023) relevant to our work. The first set of conditions involves what values of f_0 and σ_0^2 are allowed for BART to contract around f_0 . A common assumption for f_0 is isotropic smoothness,

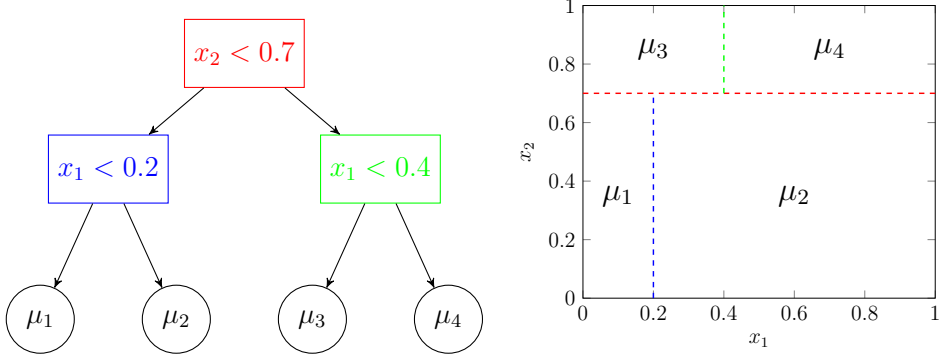


Figure 2: An example tree shown graphically (left) and as a piecewise-constant regression function (right) on the input space $[0, 1]^2$.

but this excludes the realistic scenario that f_0 is discontinuous and has different degrees of smoothness in different directions and regions. Jeong and Rockova (2023) introduce a new class of *piecewise heterogeneous anisotropic* functions whose domain is partitioned into many boxes (i.e. hyperrectangles), each of which has its own anisotropic smoothness with the same harmonic mean. First assume f_0 is d -sparse, i.e. there exists a function $h_0: [0, 1]^d \rightarrow \mathbb{R}$ and a subset $S_0 \subseteq [p]$ with $|S_0| = d$ such that $f_0(\mathbf{x}) = h_0(\mathbf{x}_{S_0})$ for any $\mathbf{x} \in [0, 1]^p$. For any given box $\Xi \subseteq [0, 1]^d$, smoothness parameter $\boldsymbol{\alpha} = (\alpha_1, \dots, \alpha_d)^T \in (0, 1]^d$, and Hölder coefficient $\lambda < \infty$, an *anisotropic $\boldsymbol{\alpha}$ -Hölder space* on Ξ is defined as

$$\mathcal{H}_\lambda^{\boldsymbol{\alpha}, d}(\Xi) := \left\{ h: \Xi \rightarrow \mathbb{R}; |h(x) - h(y)| \leq \lambda \sum_{j=1}^d |x_j - y_j|^{\alpha_j}, x, y \in \Xi \right\}.$$

Though h_0 might have different anisotropic smoothness on different boxes, it is important to assume that all boxes have the same harmonic mean. Thus define the set $\mathcal{A}_{\bar{\alpha}}^{R, d}$ to be the set of R -tuples of smoothness parameters that have harmonic mean $\bar{\alpha} \in (0, 1]$:

$$\mathcal{A}_{\bar{\alpha}}^{R, d} := \left\{ (\boldsymbol{\alpha}_1, \dots, \boldsymbol{\alpha}_R) : \boldsymbol{\alpha}_r \in (0, 1]^d, \bar{\alpha}^{-1} = p^{-1} \sum_{j=1}^d \alpha_{rj}^{-1}, r \in [R] \right\}.$$

Given a partition (Ξ_1, \dots, Ξ_R) of $[0, 1]^d$ with boxes $\Xi_r \subseteq [0, 1]^d$ and a smoothness R -tuple $A_{\bar{\alpha}} \in \mathcal{A}_{\bar{\alpha}}^{R, d}$ for some $\bar{\alpha} \in (0, 1]$, define a *piecewise heterogeneous anisotropic Hölder space* as

$$\mathcal{H}_\lambda^{A_{\bar{\alpha}}, d}(\mathfrak{X}) := \left\{ h: [0, 1]^d \rightarrow \mathbb{R}; h|_{\Xi_r} \in \mathcal{H}_\lambda^{\boldsymbol{\alpha}_r, d}(\Xi_r), r \in [R] \right\}.$$

To extend a function from a sparse domain to the original domain $[0, 1]^p$, for any nonempty subset $S \subseteq [p]$ define $W_S^p: \mathcal{C}(\mathbb{R}^{|S|}) \rightarrow \mathcal{C}(\mathbb{R}^p)$ as the map that extends $h \in \mathcal{C}(\mathbb{R}^{|S|})$ to the function $W_S^p h: \mathbf{x} \rightarrow h(\mathbf{x}_S)$ where $\mathbf{x} \in [0, 1]^p$ and $\mathcal{C}(E)$ denotes the class of real-valued continuous functions defined on a Euclidean subspace E . With this definition, the space $\mathcal{H}_\lambda^{A_{\bar{\alpha}}, d}(\mathfrak{X})$ from the preceding panel can be extended to the corresponding d -sparse *piecewise heterogeneous anisotropic Hölder space*

$$\Gamma_\lambda^{A_{\bar{\alpha}}, d, p}(\mathfrak{X}) := \bigcup_{S \subseteq [p]: |S|=d} W_S^p \left(\mathcal{H}_\lambda^{A_{\bar{\alpha}}, d}(\mathfrak{X}) \right).$$

With these definitions, we can now state the needed assumptions on the true f_0 and σ^2 .

(A1) For $d > 0$, $\lambda > 0$, $R > 0$, $\mathfrak{X} = (\Xi_1, \dots, \Xi_R)$, and $A_{\bar{\alpha}} \in \mathcal{A}_{\bar{\alpha}}^{R,d}$ with $\bar{\alpha} \in (0, 1]$, the true function satisfies $f_0 \in \Gamma_{\lambda}^{A_{\bar{\alpha}}, d, p}(\mathfrak{X})$ or $f_0 \in \Gamma_{\lambda}^{A_{\bar{\alpha}}, d, p}(\mathfrak{X}) \cap \mathcal{C}([0, 1]^p)$.

(A2) It is assumed that d, p, λ, R , and $\bar{\alpha}$ satisfy $\epsilon_n \ll 1$, where

$$\epsilon_n := \sqrt{\frac{d \log p}{n}} + (\lambda d)^{d/(2\bar{\alpha}+d)} \left(\frac{R \log n}{n} \right)^{\bar{\alpha}/(2\bar{\alpha}+d)}. \quad (4)$$

(A3) The true function f_0 satisfies $\|f_0\|_{\infty} \lesssim \sqrt{\log n}$.

(A4) The true variance parameter satisfies $\sigma^2 \in [C_0^{-1}, C_0]$ for some sufficiently large $C_0 > 1$.

2.1.2 Split-net

The second set of conditions (of the theorems of Jeong and Rockova (2023) relevant to our work) involves the split values c allowed in the binary split rules “ $x_j < c$ ” of the regression trees (again, see Figure 2 for an illustration). If a partition of $[0, 1]^p$ can be created using the aforementioned tree-based procedure, call it a *flexible tree partition*. To restrict a flexible tree partition by a set of allowable split values in the binary split rules, for any integer b_n define a *split-net* \mathcal{Z} to be a finite set of points in $[0, 1]^p$ at which possible splits occur along coordinates. That is, the allowable split values for any input dimension $j \in [p]$ are the j th components of the points in the split-net. For a given split-net \mathcal{Z} , a flexible tree partition $(\Omega_1, \dots, \Omega_K)$ of $[0, 1]^p$ with boxes $\Omega_k \subseteq [0, 1]^p$, $k \in [K]$, is called a \mathcal{Z} -tree partition if every split occurs at points in \mathcal{Z} .

A split net should be dense enough for a resulting partition to be close enough to the underlying partition $\mathfrak{X}^* = (\Xi_1^*, \dots, \Xi_R^*)$ of the true function f_0 . For any two box partitions $\mathfrak{Y}^1 = (\Psi_1^1, \dots, \Psi_J^1)$ and $\mathfrak{Y}^2 = (\Psi_1^2, \dots, \Psi_J^2)$ with the same number J of boxes, their closeness will be measured using the Hausdorff-type divergence

$$\Upsilon(\mathfrak{Y}^1, \mathfrak{Y}^2) := \min_{\tau \in \text{Perm}[J]} \max_{r \in [J]} \text{Haus}(\Psi_r^1, \Psi_{\tau(r)}^2)$$

where $\text{Perm}[J]$ denotes the set of all permutations of $[J]$ and $\text{Haus}(\cdot, \cdot)$ is the Hausdorff distance. For a subset $S \subseteq [p]$, a box partition of $[0, 1]^p$ is called *S-chopped* if every box Ψ in the box partition satisfies $\max_{j \in S} \text{len}([\Psi]_j) < 1$ and $\min_{j \notin S} \text{len}([\Psi]_j) = 1$, where $[\Psi]_j$ denotes the interval created by projecting the box $[\Psi]$ onto the j -th principal axis. For a given subset $S \subseteq [p]$, consider an *S-chopped* partition \mathfrak{Y} of $[0, 1]^p$ with J boxes. For any given $c_n \geq 0$, a split-net \mathcal{Z}_n is said to be (\mathfrak{Y}, c_n) -dense if there exists an *S-chopped* \mathcal{Z}_n -tree partition \mathcal{T}_n of $[0, 1]^p$ with J boxes such that $\Upsilon(\mathfrak{Y}, \mathcal{T}_n) \leq c_n$.

A split net should also be regular enough (defined below) for a tree partition to capture local features of f_0 on each box. Assume the underlying partition \mathfrak{X}^* can be approximated well by an $S(\mathfrak{X}^*)$ -chopped \mathcal{Z} -tree partition $(\Omega_1^*, \dots, \Omega_R^*) := \arg \min_{\mathcal{T} \in \mathcal{T}_{S(\mathfrak{X}^*), R, \mathcal{Z}}} \Upsilon(\mathfrak{X}^*, \mathcal{T})$. In each box Ω_r^* , the idea is to allow splits to occur more often along the input dimensions with less smoothness. Given a split-net \mathcal{Z} and splitting coordinate j , define the *midpoint-split* of a box Ψ as the bisection of Ψ along coordinate j at the $\lceil \tilde{b}_j(\mathcal{Z}, \Psi)/2 \rceil$ th split-candidate in $[\mathcal{Z}]_j \cap \text{int}([\Psi]_j)$, where $\tilde{b}_j(\mathcal{Z}, \Psi)$ is the cardinality of $[\mathcal{Z}]_j \cap \text{int}([\Psi]_j)$. Given a smoothness vector $\boldsymbol{\alpha} \in (0, 1]^d$, box $\Psi \subseteq [0, 1]^p$, split-net \mathcal{Z} , integer $L > 0$, and index set $S = \{s_1, \dots, s_d\} \subseteq [p]$, define the *anisotropic k-d tree AKD* $\text{AKD}(\Psi; \mathcal{Z}, \boldsymbol{\alpha}, L, S)$ as the iterative splitting procedure that partitions Ψ into disjoint boxes $\Omega_1^{\circ}, \dots, \Omega_{2^L}^{\circ}$ as follows:

1. Set $\Omega_1^\circ = \Psi$ and set counter $l_j = 0$ for each $j \in [d]$.
2. Let $L^\circ = \sum_{j=1}^d l_j$ for the current counters. For splits at iteration $1 + L^\circ$, choose $j' = \min\{\arg \min_j l_j \alpha_j\}$. Midpoint-split all boxes $\Omega_1^\circ, \dots, \Omega_{2^{L^\circ}}^\circ$ with the given \mathcal{Z} and splitting coordinate $s_{j'}$. Relabel the generated new boxes as $\Omega_1^\circ, \dots, \Omega_{2^{1+L^\circ}}^\circ$, and then increment $l_{j'}$ by one.
3. Repeat step 2 until either the updated L° equals L or the midpoint-split is no longer available. Return counters l_1, \dots, l_d and boxes $\Omega_1^\circ, \dots, \Omega_{2^{L^\circ}}^\circ$.

For a given box $\Psi \subseteq [0, 1]^p$, smoothness vector $\boldsymbol{\alpha} \in (0, 1]^d$, integer $L > 0$, and index set $S = \{s_1, \dots, s_d\} \subseteq [p]$, a split-net \mathcal{Z} is called $(\Psi, \boldsymbol{\alpha}, L, S)$ -regular if the counters and boxes returned by $AKD(\Psi; \mathcal{Z}, \boldsymbol{\alpha}, L, S)$ satisfy $L^\circ = L$ and $\max_k \text{len}([\Omega_k]_{s_j}) \lesssim \text{len}([\Psi]_{s_j}) 2^{-l_j}$ for every $j \in [d]$.

With these definitions, we can now state the needed assumptions on the sequence $\{\mathcal{Z}_n\}_{n=1}^\infty$ of split-nets.

(A5) Each split-net \mathcal{Z}_n satisfies $\max_{1 \leq j \leq p} \log b_j(\mathcal{Z}_n) \lesssim \log n$, where $b_j(\mathcal{Z}_n)$ is the cardinality of the set $\{z_j : (z_1, \dots, z_p) \in \mathcal{Z}_n\}$.

(A6) Each split-net \mathcal{Z}_n is suitably dense and regular to construct a \mathcal{Z}_n -tree partition $\hat{\mathcal{T}}$ such that there exists a simple function $\hat{f}_0 \in \mathcal{F}_{\hat{\mathcal{T}}}$ satisfying $\|f_0 - \hat{f}_0\|_n \lesssim \bar{\epsilon}_n$, where

$$\bar{\epsilon}_n := (\lambda d)^{d/(2\bar{\alpha}+d)} ((R \log n)/n)^{\bar{\alpha}/(2\bar{\alpha}+d)}, \quad (5)$$

the empirical L_2 -norm $\|\cdot\|_n$ is defined as $\|f\|_n^2 = n^{-1} \sum_{i=1}^n |f(\mathbf{x}_i)|^2$, and $\mathcal{F}_{\hat{\mathcal{T}}}$ is the set of functions on $[0, 1]^p$ that are constant on each piece of the partition $\hat{\mathcal{T}}$.

(A7) Each \mathcal{Z}_n -tree partition $(\Omega_1^*, \dots, \Omega_R^*)$ approximating the underlying partition \mathfrak{X}^* for the true function f_0 satisfies $\max_{r \in [R]} \text{depth}(\Omega_r^*) \lesssim \log n$, where depth means the depth of a node (i.e. number of nodes in the path from that node to the root node).

Finally, we state the required prior specification.

(P1) Each tree partition in the ensemble is independently assigned a tree prior with Dirichlet sparsity from Linero (2018). This sparse Dirichlet prior places a Dirichlet prior on the proportion vector used to select the splitting coordinate j during the creation of a split rule.

(P2) The step-heights of the regression-tree functions are each assigned a normal prior with mean zero and covariance matrix whose eigenvalues are bounded below and above.

(P3) The variance parameter σ^2 is assigned an inverse gamma prior.

Jeong and Rockova (2023) make the above assumptions and prior specification for their contraction-rate results in the fixed design setting (1). For their contraction-rate results in the random design setting (2), a few of the above assumptions and prior specifications are replaced by the following:

(A3*) The true function f_0 satisfies $\|f_0\|_\infty \leq C_0^*$ for some sufficiently large $C_0^* > 0$.

- (A6*) The split-net \mathcal{Z} is suitably dense and regular to construct a \mathcal{Z} -tree partition $\hat{\mathcal{T}}$ such that there exists $\hat{f}_0 \in \mathcal{F}_{\hat{\mathcal{T}}}$ satisfying $\|f_0 - \hat{f}_0\| \lesssim \bar{\epsilon}_n$ where $\bar{\epsilon}_n$ is given by (5).
- (P2*) A prior on the compact support $[-\bar{C}_1, \bar{C}_1]$ is assigned to the step-heights of the regression-tree functions for some $\bar{C}_1 > C_0^*$.
- (P3*) A prior on the compact support $[\bar{C}_2^{-1}, \bar{C}_2]$ is assigned to the variance parameter σ^2 for some $\bar{C}_2 > C_0$.

2.2 Sobol' indices

Sobol' (1990, 1993) shows that if the random variable \mathbf{X} follows an orthogonal distribution whose support is $[0, 1]^p$ and if $f \in L^2$, then the variance of $f(\mathbf{X})$ can be decomposed into a sum of terms attributed to single inputs or to interactions between sets of inputs:

$$\mathbb{V}f(\mathbf{X}) = \sum_{j=1}^p V_j + \sum_{j=1}^p \sum_{k < j} V_{jk} + \cdots + V_{1,2,\dots,p} \quad (6)$$

where we recursively define for each variable index set $P \subseteq [p]$

$$V_P := \mathbb{V}(\mathbb{E}[f(\mathbf{X}) \mid \mathbf{X}_P]) - \sum_{Q \subset P} V_Q$$

where we set $V_\emptyset = 0$ and the relation \subset denotes a strict subset. For any variable index $j \in [p]$, the term $V_{\{j\}} = V_j$ is known as the j th (unnormalized) first-order (or main-effect) Sobol' index, and the sum $T_j = \sum_{P \subseteq ([p] \setminus \{j\})} V_{P \cup \{j\}}$ is known as the j th (unnormalized) total-effect Sobol' index. We note that $T_j \geq V_j \geq 0$ for all $j \in [p]$.

The V_P terms in (6) are often divided by the total variance to produce the normalized terms $V_P / [\mathbb{V}f(\mathbf{X})]$, which have the nice interpretation of being the proportion of the total variance attributed to the interaction between the variables whose indices are in the index set P . If P is the singleton $\{j\}$, then the normalized term $V_j / [\mathbb{V}f(\mathbf{X})]$ can be interpreted as the proportion of the total variance attributed to variable j by itself. Despite this nice interpretation, the remainder of the article will assume that such indices are unnormalized unless otherwise stated.

To see why these indices' interpretation requires \mathbf{X} to follow an orthogonal distribution, we extend the definition of V_P by removing the orthogonality assumption. That is, we allow \mathbf{X} to follow a possibly non-orthogonal distribution π whose support is $[0, 1]^p$. We first define the functional $c_{P,\pi} : L^2 \rightarrow \mathbb{R}$ as

$$c_{P,\pi}(f) = \mathbb{V}_\pi(\mathbb{E}_\pi[f(\mathbf{X}) \mid \mathbf{X}_P]) = \mathbb{E}_\pi[(\mathbb{E}_\pi[f(\mathbf{X}) \mid \mathbf{X}_P])^2] - [\mathbb{E}_\pi f(\mathbf{X})]^2 \quad (7)$$

for any $f \in L^2$. Then the generalized V_P under the distribution π is recursively defined as

$$V_{P,\pi}(f) := c_{P,\pi}(f) - \sum_{Q \subset P} V_{Q,\pi}(f),$$

where again we set $V_{\emptyset,\pi}(f) = 0$. Similarly, we define the generalized j th total-effect term:

$$T_{j,\pi}(f) = \sum_{P \subseteq ([p] \setminus \{j\})} V_{P \cup \{j\},\pi}(f)$$

where the binary relation \subseteq denotes a subset that is not necessarily strict. Recall that if π is orthogonal and $f \in L^2$, then $T_{j,\pi}(f) \geq V_{j,\pi}(f) \geq 0$ for all $j \in [p]$ and the variance decomposition (6) (where orthogonality implies $V_P = V_{P,\pi}(f)$ for all $P \subseteq [p]$) holds. However, Theorem 2 of Song et al. (2016) asserts the existence of a non-orthogonal distribution π and a function $f \in L^2$ such that $\sum_{j=1}^p V_{j,\pi}(f) > \mathbb{V}_\pi f(\mathbf{X}) > \sum_{j=1}^p T_{j,\pi}(f)$. In such a case, these Sobol' indices can no longer be interpreted as in the orthogonal case.

2.3 Shapley effects

One way to measure variable activity, regardless of dependence among inputs, are the Shapley effects defined by Song et al. (2016) as the Shapley values in Owen (2014) using the functional (7) as the “value” or “cost.” For $j \in [p]$ the j th Shapley effect is defined as

$$S_{j,\pi}(f) = (p!)^{-1} \sum_{P \subseteq ([p] \setminus \{j\})} (p - |P| - 1)! |P|! [c_{P \cup \{j\}, \pi}(f) - c_{P, \pi}(f)], \quad (8)$$

which has the desirable property $\sum_{j=1}^p S_{j,\pi}(f) = \mathbb{V}_\pi f(\mathbf{X})$ for any distribution π (possibly nonorthogonal) whose support is $[0, 1]^p$. Hence, the j th Shapley effect (after normalization) can be nicely interpreted as the contribution of input j to the total output variance. Furthermore, if π is orthogonal, then

$$V_{j,\pi}(f) \leq S_{j,\pi}(f) \leq T_{j,\pi}(f) \quad (9)$$

for any $f \in L^2$ and $j \in [p]$ (Owen, 2014, Section 3), i.e. the j th Shapley effect is bounded between the j th main-effect and total-effect Sobol' index.

Calculating (8) can be prohibitively costly due to it being a sum of values (7) over all subsets of a set $[p] \setminus \{j\}$. Its computational tractability will be discussed in Section 4.

3 Posterior asymptotics

This section establishes our contraction-rate results (Corollaries 1 and 2) for estimators of Sobol' indices and Shapley effects under either the fixed design (1) or the random design (2). Our proofs rely on these sensitivity indices having a property (defined in Lemma 1 below) similar to but slightly less restrictive than Lipschitz continuity. However, the tasks of proving this property for all of these sensitivity indices are very similar to each other. Because these indices are linear combinations of the functional $c_{P,\pi}$ defined in (7), we can use Lemma 1 to reduce the above tasks to the single task of proving this property for $c_{P,\pi}$.

Lemma 1. *Suppose the following relationship is true for all indices k in a finite set \mathcal{A} : given two metric spaces X and X_0 with the same metric d_X , there exists a constant $C > 0$ such that, for all $(x, x_0) \in X \times X_0$, the function $\phi_k: X \cup X_0 \rightarrow \mathbb{R}$ satisfies*

$$|\phi_k(x) - \phi_k(x_0)| \leq C d_X(x, x_0).$$

Then any set $\{a_k\}_{k \in \mathcal{A}}$ of real numbers satisfies

$$\left| \sum_{k \in \mathcal{A}} a_k \phi_k(x) - \sum_{k \in \mathcal{A}} a_k \phi_k(x_0) \right| \leq C^* d_X(x, x_0).$$

where $C^ = C \sum_{k \in \mathcal{A}_+} |a_k|$ and $\mathcal{A}_+ := \{k \in \mathcal{A}: |\phi_k(x) - \phi_k(x_0)| > 0\}$.*

3.1 Nonparametric regression with random design

This section assumes the random-design regression setting (2); all expectations in this section are with respect to the probability measure π in (2).

Theorem 1. *Assume (A3*). If $f \in L^2([0, 1]^p)$ shares the same bound C_0^* from (A3*), then for any subset $P \subseteq [p]$ and distribution π with support $[0, 1]^p$ we have*

$$|c_{P,\pi}(f) - c_{P,\pi}(f_0)| \leq 4C_0^* \|f - f_0\|_{2,\pi}$$

for the functional $c_{P,\pi}$ defined in (7).

Corollary 1. *Under the assumptions of Theorem 4 of Jeong and Rockova (2023) – Assumptions (A1), (A2), (A3*), (A4), (A5), (A6*), and (A7), and the prior assigned through (P1), (P2*), and (P3*) – and Theorem 1 above, there exist positive constants $L_{V,\pi,|P|}$, $L_{T,\pi}$, and L_S such that as $n \rightarrow \infty$ for ϵ_n in (4),*

$$\begin{aligned} \mathbb{E}_0 \Pi \left\{ (f, \sigma^2) : |V_{P,\pi}(f) - V_{P,\pi}(f_0)| + |\sigma^2 - \sigma_0^2| > L_{V,\pi,|P|} \epsilon_n \middle| Y_1, \dots, Y_n \right\} &\rightarrow 0, \\ \mathbb{E}_0 \Pi \left\{ (f, \sigma^2) : |T_{j,\pi}(f) - T_{j,\pi}(f_0)| + |\sigma^2 - \sigma_0^2| > L_{T,\pi} \epsilon_n \middle| Y_1, \dots, Y_n \right\} &\rightarrow 0, \\ \text{and } \mathbb{E}_0 \Pi \left\{ (f, \sigma^2) : |S_{j,\pi}(f) - S_{j,\pi}(f_0)| + |\sigma^2 - \sigma_0^2| > L_S \epsilon_n \middle| Y_1, \dots, Y_n \right\} &\rightarrow 0. \end{aligned}$$

3.2 Nonparametric regression with fixed design

This section assumes the fixed-design regression setting (1); all expectations in this section are with respect to the probability measure $P_{\mathcal{X}}(\cdot) = n^{-1} \sum_{\mathbf{x} \in \mathcal{X}} \delta_{\mathbf{x}}(\cdot)$ where \mathcal{X} is the set of the fixed covariates assumed in (1).

Theorem 2. *Assume (A3). If $f \in L^2([0, 1]^p)$ shares the same bound $\sqrt{\log n}$ from (A3), then for any subset $P \subseteq [p]$ and distribution π with support $[0, 1]^p$ we have*

$$|c_{P,P_{\mathcal{X}}}(f) - c_{P,P_{\mathcal{X}}}(f_0)| \lesssim 4\sqrt{\log n} \|f - f_0\|_{2,P_{\mathcal{X}}}$$

where the empirical L_2 -norm $\|\cdot\|_{2,P_{\mathcal{X}}}$ is defined as $\|f\|_{2,P_{\mathcal{X}}}^2 = n^{-1} \sum_{\mathbf{x} \in \mathcal{X}} |f(\mathbf{x})|^2$.

Corollary 2. *Under the assumptions of Theorem 2 of Jeong and Rockova (2023) – Assumptions (A1), (A2), (A3), (A4), (A5), (A6), and (A7), and the prior assigned through (P1), (P2), and (P3) – and Theorem 2 above, there exist positive constants $L_{V,\pi,|P|}$, $L_{T,\pi}$, and L_S such that as $n \rightarrow \infty$ for ϵ_n in (4),*

$$\begin{aligned} \mathbb{E}_0 \Pi \left\{ (f, \sigma^2) : |V_{P,\pi}(f) - V_{P,\pi}(f_0)| + |\sigma^2 - \sigma_0^2| > L_{V,\pi,|P|} \epsilon_n \sqrt{\log n} \mid Y_1, \dots, Y_n \right\} &\rightarrow 0, \\ \mathbb{E}_0 \Pi \left\{ (f, \sigma^2) : |T_{j,\pi}(f) - T_{j,\pi}(f_0)| + |\sigma^2 - \sigma_0^2| > L_{T,\pi} \epsilon_n \sqrt{\log n} \mid Y_1, \dots, Y_n \right\} &\rightarrow 0, \\ \text{and } \mathbb{E}_0 \Pi \left\{ (f, \sigma^2) : |S_{j,\pi}(f) - S_{j,\pi}(f_0)| + |\sigma^2 - \sigma_0^2| > L_S \epsilon_n \sqrt{\log n} \mid Y_1, \dots, Y_n \right\} &\rightarrow 0. \end{aligned}$$

4 Computation of Shapley effects

This section considers the computational tractability of estimating Shapley effects of the regression function f_0 for various fitted Bayesian surrogate models, each summarized by n_{draw} posterior draws. For each draw i , let $\hat{f}^{(i)}$ be the i th surrogate regression function. For each input $j \in [p]$, we can estimate the j th Shapley effect $S_{j,\pi}(f_0)$ of f_0 by computing and then averaging the n_{draw} values of $S_{j,\pi}(\hat{f}^{(i)})$:

$$\begin{aligned} S_{j,\pi}(f_0) &\approx n_{draw}^{-1} \sum_{i=1}^{n_{draw}} S_{j,\pi}(\hat{f}^{(i)}) \\ &= n_{draw}^{-1} \sum_{i=1}^{n_{draw}} (p!)^{-1} \sum_{P \subseteq ([p] \setminus \{j\})} (p - |P| - 1)! |P|! [c_{P \cup \{j\}, \pi}(\hat{f}^{(i)}) - c_{P, \pi}(\hat{f}^{(i)})]. \end{aligned}$$

But for each $\hat{f}^{(i)}$, computing the p Shapley effects would require computing the cost function (7) for 2^p subsets of the set $[p]$. This approach for all inputs would thus require $n_{draw} \times 2^p$ computations of (7). The exponential increase in p is undesirable, but also the calculation of even a single cost function might be computationally intractable if p is large enough.

We first tackle the exponential increase in p . To reduce the increase from exponential to linear, Song et al. (2016); Broto et al. (2020) use a permutation-based approach, but we use the following random-subset approach. For some chosen positive integer m and each posterior draw i and input $j \in [p]$, do the following m times: randomly draw a subset $P \subseteq ([p] \setminus \{j\})$ by including each $j' \in ([p] \setminus \{j\})$ in P with probability 0.5 (which gives each subset of $([p] \setminus \{j\})$ equal probability 2^{1-p} of being chosen), then compute the difference $c_{P \cup \{j\}, \pi}(\hat{f}^{(i)}) - c_{P, \pi}(\hat{f}^{(i)})$ for the randomly drawn subset P . Then construct point estimates and credible intervals for the Shapley effect $S_{j,\pi}(f_0)$ using the n_{draw} values

$$m^{-1} \sum_{l=1}^m [c_{P_l^{(i)} \cup \{j\}, \pi}(\hat{f}^{(i)}) - c_{P_l^{(i)}, \pi}(\hat{f}^{(i)})], \quad i = 1, 2, \dots, n_{draw} \quad (10)$$

where $P_l^{(i)}$ is the l th of m randomly drawn subset of $([p] \setminus \{j\})$ for the i th posterior draw. For example, a point estimate for $S_{j,\pi}(f_0)$ could be constructed by taking the sample mean of the n_{draw} values in (10), and a 95% credible interval can be constructed by using the end points of the middle 95% values in (10), though we note that such credibles are likely inflated due to the additional variability from the random subsets. Hence this approach reduces the number of cost-function calculations from $n_{draw} \times 2^p$ to $n_{draw} \times p \times (2m)$.

What value of m should be used? Both the computational cost and the accuracy of the surrogate-based Shapley-effect estimate increase with $m \times n_{draw}$. Because $n_{draw} \gg 1$ for any decent posterior summary of the surrogate model, we consider using a small value of m to keep the computational cost reasonable. For the remainder of the article, we prioritize keeping computational cost low and hence use $m = 1$.

(Alternatively, if the inputs are orthogonal, we could get a rough sense of the posterior uncertainty of the Shapley-effect estimate by exploiting the relationship (9), which bounds a CI length for a Shapley effect by the CI lengths of the two Sobol' indices.)

We now consider how each calculation of (7) is affected by which surrogate is used. If the integrals in (7) have a closed-form expression, they can be computed exactly. For

BART, a closed-form expression can be found using Theorem 1 of Horiguchi et al. (2021). For Bayesian MARS, Francom et al. (2018) provides a closed-form expression for estimating Sobol' indices and contains a numerical example with $p = 200$. For a GP, a closed-form expression can be found for certain correlation functions, but these functions are typically restrictive i.e., assume stationarity and isotropy. If the closed form is unavailable, the integrals can be approximated but the computation time will likely grow superlinearly in p to keep the resulting integral approximation error small. See Table 1 for a summary.

5 Numerical examples

5.1 $d = 5$ active input variables

This section explores the performance of BART-based Shapley effects for $d = 5$ active variables. (BART-based Sobol' indices are evaluated in detail in Horiguchi et al. (2021) and Horiguchi (2020) and hence is not evaluated in this paper.) Datasets are generated using the following four test functions, for which Table 2 in the Supplementary Materials contains the variances, Sobol' indices, and Shapley values:

1. The “Friedman” function (Friedman, 1991) is defined as

$$f(\mathbf{x}) := 10 \sin(\pi x_1 x_2) + 20(x_3 - 0.5)^2 + 10x_4 + 5x_5.$$

2. The “Morris” function inspired by Morris et al. (2006) is defined as

$$f(\mathbf{x}) := \alpha \sum_{i=1}^d x_i + \beta \sum_{i=1}^{d-1} x_i \sum_{j=i+1}^d x_j$$

where $\alpha = \sqrt{12} - 6\sqrt{0.1(d-1)} \approx -0.331$ and $\beta = \frac{12}{\sqrt{10(d-1)}} \approx 1.897$ are chosen.

3. The “Bratley” function (Bratley et al., 1992; Kucherenko et al., 2011) is defined as

$$f(\mathbf{x}) := \sum_{i=1}^d (-1)^i \prod_{j=1}^i x_j = -x_1 + x_1 x_2 - x_1 x_2 x_3 + x_1 x_2 x_3 x_4 - x_1 x_2 x_3 x_4 x_5.$$

4. The “ g -function” from Saltelli and Sobol' (1995) is defined as

$$f(\mathbf{x}) := \prod_{k=1}^d \frac{|4x_k - 2| + c_k}{1 + c_k},$$

where we use $c_k = (k-1)/2$ for $k = 1, \dots, d$ suggested by Crestaux et al. (2009).

For our first set of experiments, we create a dataset with $n = 50p$ observations and noise variance $\sigma_0^2 = 0.25Var(f(\mathbf{X}))$ from (1) for each test function f and each $p \in \{5, 50, 200\}$. To each dataset, we fit a BART model with $n_{draw} = 1000$ posterior draws and 200 trees with code from Pratola (2023). For comparison, we also fit a Gaussian process (GP) model using `shapleyPermRand`, which was the only function in the `sensitivity` R package (Iooss

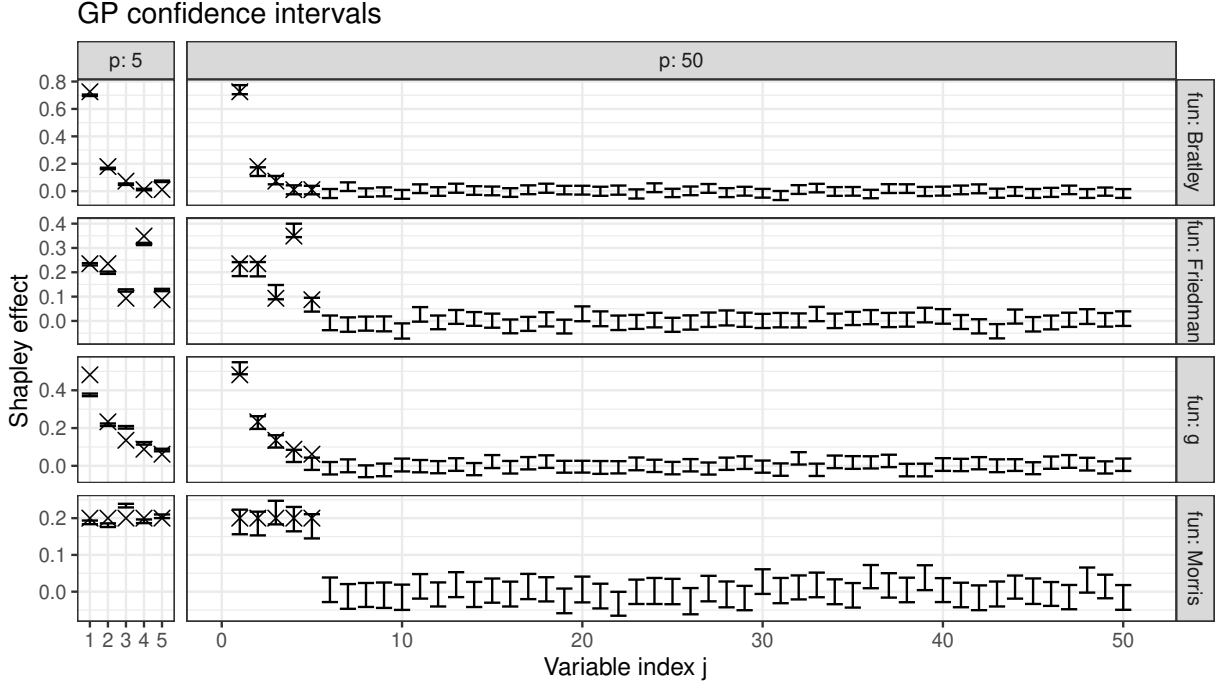


Figure 3: 95% confidence intervals (as computed by `sensitivity`) for the Shapley-effect estimates from a GP model fit to $n = 50p$ observations with $d = 5$ active variables. Crosses indicate function's true Shapley effects. The `shapleyPermRand` approach samples $N_V + m(p-1)N_O N_I$ inputs to estimate expectation. As recommended by Song et al. (2016), we set $N_V = 10^5$ samples to estimate the total variance, and we set $N_O = 1$ and $N_I = 3$ to estimate the outer and inner expectations, respectively. For $p = 5$ we use $m = 10^5$ random permutations; for $p = 50$ we reduce this to $m = 3 \times 10^3$ to avoid numerical overflow.

et al., 2023) that we found could fit to our $p = 50$ data sets in a reasonable amount of time. Parameter specifications are in the caption of Figure 3. For the $p = 200$ cases, we could not read the large GP-model file sizes into R and hence do not include these results.

We first compare the GP estimates to the BART estimates. Figure 3 shows the Shapley-effect confidence intervals of the GP approach as computed by the `sensitivity` package, and Figure 4 shows our Shapley-effect credible intervals using BART as defined in (10). The GP model seems to capture the large Shapley effects better than the BART model does, which might be explained by the fact that the data-generating functions are all continuously differentiable and thus are well suited for GPs. However, the GP model also seems to have more trouble setting the inactive variables to have zero estimated Shapley effect; indeed, for the g -function with $p = 50$, the confidence intervals for many of the inactive variables are higher than the interval for the active variable $j = 5$. Furthermore, the GP confidence intervals for all *inactive* variables cover negative values (as computed by the `sensitivity` package), even though Shapley effects are nonnegative by definition. In contrast, the BART credible intervals never cover negative values.

We further examine the BART results in Figure 4. For the Friedman and Morris functions, the true Shapley effects are contained in the credible intervals and are often near the center of the intervals. For the g -function, the $p = 5$ scenario shows the credible intervals struggling a bit to capture the true Shapley effects, but the $p = 200$ scenarios show

BART credible intervals

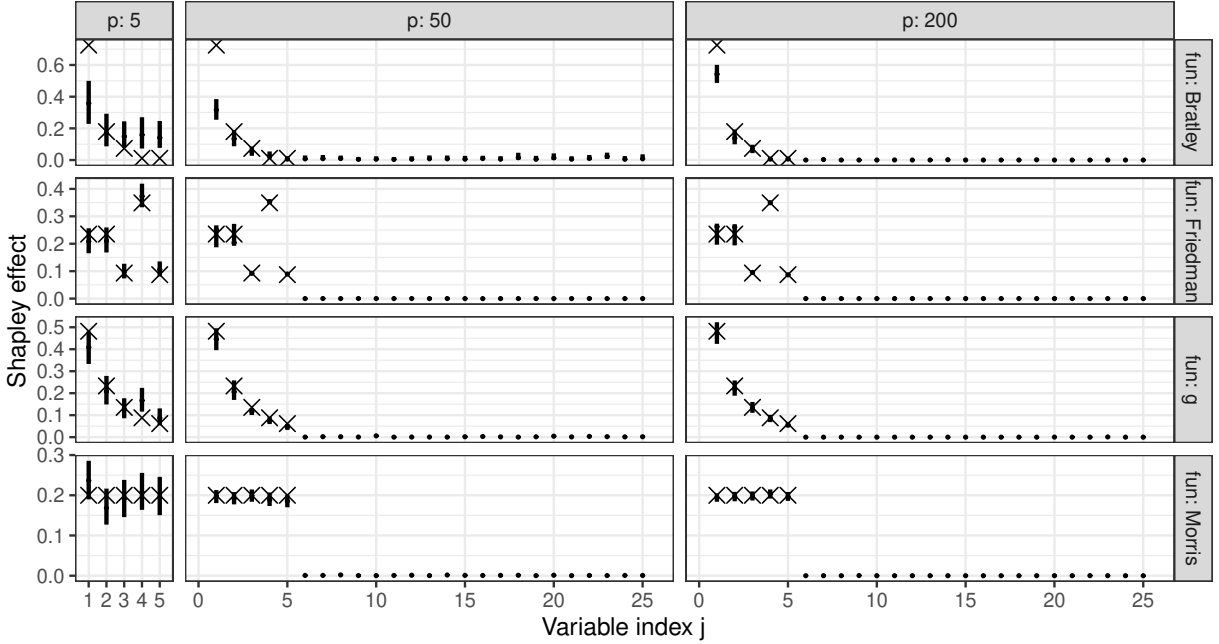


Figure 4: 95% credible intervals (as computed in (10)) over 1000 posterior draws for the Shapley-effect estimates from a BART model fit to $n = 50p$ observations with $d = 5$ active variables. Crosses correspond to function’s true Shapley effects. For $p = 50$ and $p = 200$, only the first 25 input variables are shown for space considerations.

better performance from the intervals. This $p = 200$ result becomes even more notable if we consider the fitted BART models do not use (P1)’s tree prior with Dirichlet sparsity from Linero (2018), and that the g function is purely a product of univariate functions. For the Bratley function, the intervals struggle quite a bit to capture the true Shapley effects. For this challenging Bratley function, we next explore what parameters or priors should be changed to improve the Shapley-effect estimates. Of the three directions we explored – increasing the number of trees to 300, weakening the tree-depth prior to encourage higher order interactions, and increasing n – only the third (with 200 trees, the same tree-depth prior as in the first set of explorations, and $p = 5$) yielded estimates closer to the true Shapley effects. This provides assurance that for these more challenging functions, the estimates can be close to the true Shapley effects if n is large enough without having to change any other parameters or priors.

5.2 $d = 250$ active input variables

This section explores the performance of BART-based Shapley effects for $d = 250$ active input variables and input dimension $p = 500$, which is a regime that bottlenecks most other methods. (We omit any GP results here due to not being able to compute GP-based Shapley-effect estimates.) For convenience we use the Morris function since its Shapley effects for the d active variables are all $1/d$. Figure 5 shows that BART clearly distinguishes between the first 250 inputs (these intervals are centered around $1/d$) and the second 250 inputs (these intervals are centered around zero) even for such a large p .

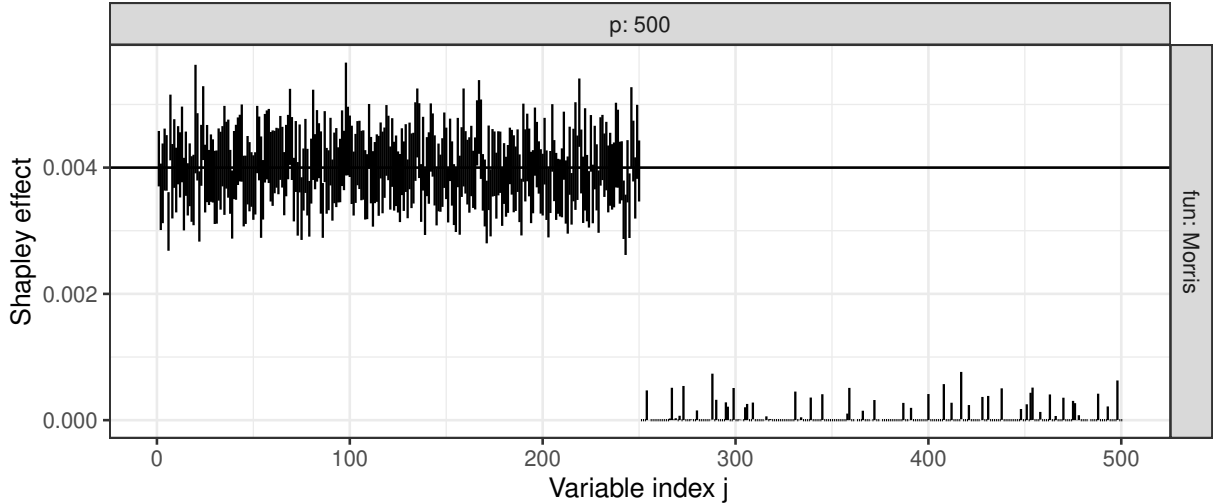


Figure 5: 95% credible intervals (as computed in (10)) over 300 posterior draws for the Shapley-effect estimates from a BART model fit to $n = 50p$ observations. Horizontal line corresponds to the function’s true Shapley effects of the $d = 250$ active variables.

5.3 Application to climate simulator

Here we estimate Shapley effects from data generated from the En-ROADS climate simulator (Climate Interactive et al., 2020). This simulator is a mathematical model of how global temperature is influenced by changes in energy, land use, consumption, agriculture, and other factors. It is designed to be easily used by the general public. The model is an ordinary differential equation solved by Euler integration and synthesizes the important drivers of climate in a computationally efficient and easy-to-use web interface.

The data consists of $n = 110$ observations with $p = 11$ inputs and was collected using the scheme described in Horiguchi et al. (2021). To this data we fit a BART model and compute Shapley-effect estimates using the implementation in Pratola (2023) with 1000 posterior draws, 200 trees, and the remaining default parameter settings.

Figure 6 shows the estimates for the first-order Sobol’ index, Shapley effect, and total-effect Sobol’ index of the 11 inputs. For each input, the relationship (9) between the three indices is shown. As expected given this relationship and the analysis in Horiguchi et al. (2021), the small differences between the Shapley-effect estimates and the two Sobol’-index estimates indicate small interaction effects between any group of inputs. Hence, the takeaways about the impact of each input are the same as discussed in Horiguchi et al. (2021). In particular, the four most impactful inputs seem to be carbon price, energy efficiency of buildings, methane, and economic growth.

6 Discussion

This article establishes posterior contraction rates for Sobol’-index and Shapley-effect estimators computed using BART. The proofs of our contraction rates required proving a property similar to Lipschitz continuity for Sobol’ indices and Shapley effects before using recent contraction-rate results that applies to function spaces with heterogeneous smooth-

Sensitivity index estimates for En-Roads climate simulator

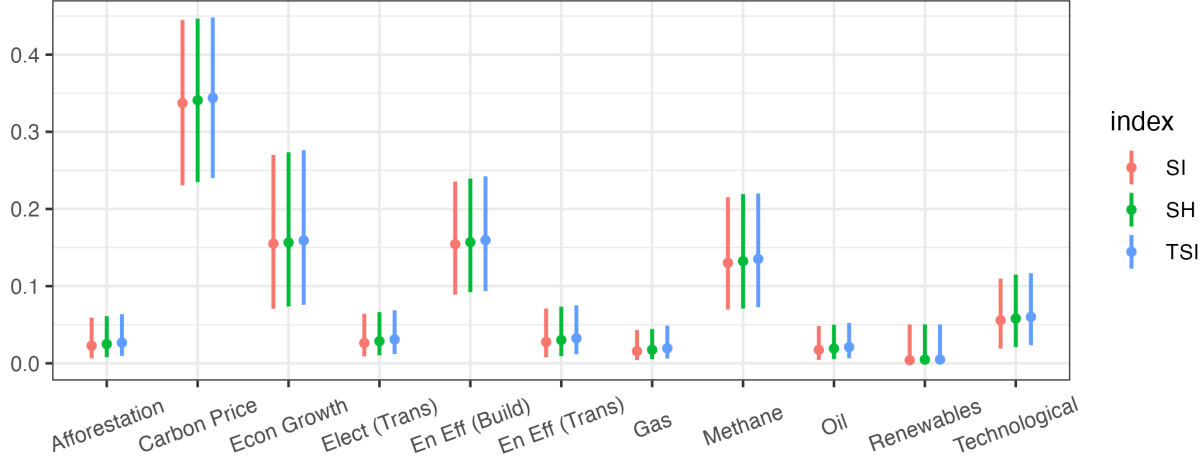


Figure 6: 95% credible intervals (as computed in (10)) for (normalized) first-order Sobol' indices (SI), Shapley effects (SH), and total-effect Sobol' indices (TSI) over 1000 posterior draws from a BART model fit to climate simulator data (Climate Interactive et al., 2020).

ness and sparsity in high dimensions and to fixed and random designs. This article also illustrates the computational tractability and performance of BART-based Shapley effects on four different test functions under orthogonal inputs and $p = 500$. Code to fit BART models and compute Sobol' index and Shapley effect estimates is found in Pratola (2023).

Regarding computation, it is challenging to encode an arbitrary (e.g. nonorthogonal) input design with full support into a BART model. This can be possibly achieved by replacing the volume of each hyperrectangle used to compute BART-based Sobol' indices and Shapley effects with the proportion of observations that fall in each hyperrectangle. A direction for future work is to implement the calculation of BART-based Shapley effects under an arbitrary (e.g. nonorthogonal) input design and evaluate its performance.

References

Benoumechiara, N. and K. Elie-Dit-Cosaque (2019). Shapley effects for sensitivity analysis with dependent inputs: bootstrap and kriging-based algorithms. *ESAIM: Proceedings and Surveys* 65, 266–293.

Bratley, P., B. L. Fox, and H. Niederreiter (1992). Implementation and tests of low-discrepancy sequences. *ACM Transactions on Modeling and Computer Simulation (TOMACS)* 2(3), 195–213.

Broto, B., F. Bachoc, and M. Depecker (2020). Variance reduction for estimation of shapley effects and adaptation to unknown input distribution. *SIAM/ASA Journal on Uncertainty Quantification* 8(2), 693–716.

Chen, W., R. Jin, and A. Sudjianto (2005). Analytical variance-based global sensitivity analysis in simulation-based design under uncertainty. *Journal of mechanical design* 127(5), 875–886.

Chen, W., R. Jin, and A. Sudjianto (2006). Analytical global sensitivity analysis and uncertainty propagation for robust design. *Journal of quality technology* 38(4), 333–348.

Chipman, H., P. Ranjan, and W. Wang (2012). Sequential design for computer experiments with a flexible Bayesian additive model. *Canadian Journal of Statistics* 40(4), 663–678.

Chipman, H. A., E. I. George, and R. E. McCulloch (2010). Bart: Bayesian additive regression trees. *The Annals of Applied Statistics* 4(1), 266–298.

Climate Interactive, Ventana Systems, Todd Fincannon, UML Climate Change Initiative, and MIT Sloan (2020). EnROADS climate change solutions simulator. <https://en-roads.climateinteractive.org/scenario.html?v=2.7.15>. Accessed: 2020-04-03.

Crestaux, T., O. L. Maître, and J.-M. Martinez (2009). Polynomial chaos expansion for sensitivity analysis. *Reliability Engineering & System Safety* 94(7), 1161 – 1172. Special Issue on Sensitivity Analysis.

Denison, D. G., B. K. Mallick, and A. F. Smith (1998). Bayesian mars. *Statistics and Computing* 8, 337–346.

Francom, D., B. Sansó, A. Kupresanin, and G. Johannesson (2018). Sensitivity analysis and emulation for functional data using bayesian adaptive splines. *Statistica Sinica* 28(2), 791–816.

Friedman, J. H. (1991). Multivariate adaptive regression splines. *The annals of statistics* 19(1), 1–67.

Ghosal, S. and A. Van der Vaart (2017). *Fundamentals of nonparametric Bayesian inference*, Volume 44. Cambridge University Press.

Goda, T. (2021). A simple algorithm for global sensitivity analysis with shapley effects. *Reliability Engineering & System Safety* 213, 107702.

Gramacy, R. B. and B. Haaland (2016). Speeding up neighborhood search in local Gaussian process prediction. *Technometrics* 58(3), 294–303.

Gramacy, R. B. and M. Taddy (2010). Categorical inputs, sensitivity analysis, optimization and importance tempering with tgp version 2, an R package for treed Gaussian process models. *Journal of Statistical Software* 33(6), 1–48.

Gramacy, R. B., M. Taddy, S. M. Wild, et al. (2013). Variable selection and sensitivity analysis using dynamic trees, with an application to computer code performance tuning. *The Annals of Applied Statistics* 7(1), 51–80.

Horiguchi, A. (2020). *Bayesian Additive Regression Trees: Sensitivity Analysis and Multi-objective Optimization*. Ph. D. thesis, The Ohio State University.

Horiguchi, A., M. T. Pratola, and T. J. Santner (2021). Assessing variable activity for bayesian regression trees. *Reliability Engineering & System Safety* 207, 107391.

Horiguchi, A., T. J. Santner, Y. Sun, and M. T. Pratola (2022). Using bart to perform pareto optimization and quantify its uncertainties. *Technometrics* 64(4), 1–11.

Iooss, B. and C. Prieur (2019). Shapley effects for sensitivity analysis with correlated inputs: comparisons with sobol' indices, numerical estimation and applications. *International Journal for Uncertainty Quantification* 9(5).

Iooss, B., S. D. Veiga, A. Janon, G. Pujol, with contributions from Baptiste Broto, K. Boumhaout, T. Delage, R. E. Amri, J. Fruth, L. Gilquin, J. Guillaume, M. Herin, M. I. Idrissi, L. Le Gratiet, P. Lemaitre, A. Marrel, A. Meynaoui, B. L. Nelson, F. Monari, R. Oomen, O. Rakovec, B. Ramos, O. Roustant, G. Sarazin, E. Song, J. Staum, R. Sueur, T. Touati, V. Verges, and F. Weber (2023). *sensitivity: Global Sensitivity Analysis of Model Outputs*. R package version 1.28.1.

Jeong, S. and V. Rockova (2023). The art of bart: Minimax optimality over nonhomogeneous smoothness in high dimension. *Journal of Machine Learning Research* 24(337), 1–65.

Kucherenko, S., B. Feil, N. Shah, and W. Mauntz (2011). The identification of model effective dimensions using global sensitivity analysis. *Reliability Engineering & System Safety* 96(4), 440–449.

Li, S., B. Yang, and F. Qi (2016). Accelerate global sensitivity analysis using artificial neural network algorithm: Case studies for combustion kinetic model. *Combustion and Flame* 168, 53–64.

Linero, A. R. (2018). Bayesian regression trees for high-dimensional prediction and variable selection. *Journal of the American Statistical Association* 113(522), 626–636.

Liu, Y., V. Ročková, and Y. Wang (2021, 04). Variable Selection with ABC Bayesian Forests. *Journal of the Royal Statistical Society Series B: Statistical Methodology* 83(3), 453–481.

Marrel, A., B. Iooss, B. Laurent, and O. Roustant (2009). Calculations of Sobol' indices for the Gaussian process metamodel. *Reliability Engineering & System Safety* 94(3), 742–751.

Mohammadi, H., P. Challenor, M. Goodfellow, and D. Williamson (2019). Emulating computer models with step-discontinuous outputs using gaussian processes. *arXiv preprint arXiv:1903.02071*.

Moon, H. (2010). *Design and analysis of computer experiments for screening input variables*. Ph. D. thesis, The Ohio State University.

Morris, M. D., L. M. Moore, and M. D. McKay (2006). Sampling plans based on balanced incomplete block designs for evaluating the importance of computer model inputs. *Journal of Statistical Planning and Inference* 136(9), 3203–3220.

Oakley, J. E. and A. O'Hagan (2004). Probabilistic sensitivity analysis of complex models: a Bayesian approach. *Journal of the Royal Statistical Society: Series B (Statistical Methodology)* 66(3), 751–769.

Owen, A. B. (2014). Sobol' indices and shapley value. *SIAM/ASA Journal on Uncertainty Quantification* 2(1), 245–251.

Plischke, E., G. Rabitti, and E. Borgonovo (2021). Computing shapley effects for sensitivity analysis. *SIAM/ASA Journal on Uncertainty Quantification* 9(4), 1411–1437.

Pratola, M. T. (2023). Open Bayesian trees. Accessed: 2023-04-03.

Radaideh, M. I. and T. Kozlowski (2020). Surrogate modeling of advanced computer simulations using deep gaussian processes. *Reliability Engineering & System Safety* 195, 106731.

Saltelli, A. and I. M. Sobol' (1995). About the use of rank transformation in sensitivity analysis of model output. *Reliability Engineering & System Safety* 50(3), 225 – 239.

Santner, T. J., B. J. Williams, and W. I. Notz (2018). *The Design and Analysis of Computer Experiments, Second Edition*. Springer-Verlag.

Shapley, L. S. (1952). A value for n-person games. Technical report, The RAND Corporation.

Sobol', I. M. (1990). On sensitivity estimation for nonlinear mathematical models. *Matematicheskoe modelirovanie* 2(1), 112–118.

Sobol', I. M. (1993). Sensitivity estimates for nonlinear mathematical models. *MMCE* 1(4), 407–414.

Song, E., B. L. Nelson, and J. Staum (2016). Shapley effects for global sensitivity analysis: Theory and computation. *SIAM/ASA Journal on Uncertainty Quantification* 4(1), 1060–1083.

Sudret, B. (2008). Global sensitivity analysis using polynomial chaos expansions. *Reliability engineering & system safety* 93(7), 964–979.

Svenson, J., T. Santner, A. Dean, and H. Moon (2014). Estimating sensitivity indices based on gaussian process metamodels with compactly supported correlation functions. *Journal of Statistical Planning and Inference* 144, 160–172.

van der Pas, S. and V. Ročková (2017). Bayesian dyadic trees and histograms for regression. In I. Guyon, U. V. Luxburg, S. Bengio, H. Wallach, R. Fergus, S. Vishwanathan, and R. Garnett (Eds.), *Advances in Neural Information Processing Systems 30*, pp. 2089–2099. Curran Associates, Inc.

Wu, Z., D. Wang, P. Okolo, F. Hu, and W. Zhang (2016). Global sensitivity analysis using a gaussian radial basis function metamodel. *Reliability Engineering & System Safety* 154, 171–179.

j	Friedman			Morris			Bratley			g -function		
	Var: 23.8			Var: 5.25			Var: 0.057			Var: 3.076		
	V_j^*	T_j^*	S_j^*	V_j^*	T_j^*	S_j^*	V_j^*	T_j^*	S_j^*	V_j^*	T_j^*	S_j^*
1	0.197	0.274	0.235	0.190	0.210	0.2	0.688	0.766	0.725	0.411	0.558	0.482
2	0.197	0.274	0.235	0.190	0.210	0.2	0.142	0.220	0.179	0.183	0.288	0.233
3	0.093	0.093	0.093	0.190	0.210	0.2	0.051	0.099	0.073	0.103	0.172	0.135
4	0.350	0.350	0.350	0.190	0.210	0.2	0.006	0.018	0.011	0.066	0.113	0.088
5	0.087	0.087	0.087	0.190	0.210	0.2	0.006	0.018	0.011	0.046	0.080	0.062

Table 2: Normalized main-effects $V_j^* = V_j^*(f)$, total-effects $T_j^* = T_j^*(f)$, and Shapley effects $S_j^* = S_j^*(f)$ for various functions f and variable indices $j \in [5]$ under orthogonal inputs.

SUPPLEMENTARY MATERIAL

A Sensitivity index values for functions in Section 5

See Table 2.

B Review of Posterior contraction

A posterior contraction rate quantifies how quickly a posterior distribution approaches the true parameter of the data's distribution. We use a simplified version of the definition from Ghosal and Van der Vaart (2017): for every $n \in \mathbb{N}$, let $X^{(n)}$ be an observation in a sample space $(\mathfrak{X}^{(n)}, \mathcal{X}^{(n)})$ with distribution $P_\theta^{(n)}$ indexed by θ belonging to a first countable topological space Θ . Given a prior Π_n on the Borel sets of Θ , let $\Pi_n(\cdot | X^{(n)})$ be (a fixed particular version of) the posterior distribution.

Definition 1 (Posterior contraction rate). *A sequence $\{\varepsilon_n\}_{n \in \mathbb{N}}$ is a posterior contraction rate at the parameter θ_0 with respect to the semimetric d if $\Pi_n(\theta: d(\theta, \theta_0) \geq M_n \varepsilon_n | X^{(n)}) \rightarrow 0$ in $P_{\theta_0}^{(n)}$ -probability, for every $M_n \rightarrow \infty$.*

If there exists a constant $M > 0$ such that $\Pi_n(\theta: d(\theta, \theta_0) \geq M \varepsilon_n | X^{(n)}) \rightarrow 0$ in $P_{\theta_0}^{(n)}$ -probability, then the sequence $\{\varepsilon_n\}_{n \in \mathbb{N}}$ satisfies the definition of posterior contraction rate. This will be relevant in interpreting Corollaries 1 and 2 in Section 3.

C Proofs

Proof of Lemma 1. We have

$$\left| \sum_{k \in \mathcal{A}} a_k \phi_k(x) - \sum_{k \in \mathcal{A}} a_k \phi_k(x_0) \right| \leq \sum_{k \in \mathcal{A}} |a_k| |\phi_k(x) - \phi_k(x_0)| \leq \sum_{k \in \mathcal{A}_+} |a_k| C d_X(x, x_0)$$

where the right-most sum in the preceding panel is exactly $C^* d_X(x, x_0)$. \square

Proof of Theorem 1. Note that

$$\begin{aligned} |c_{P,\pi}(f) - c_{P,\pi}(f_0)| &= \left| \left(\mathbb{E}[(\mathbb{E}[f(\mathbf{X}) \mid \mathbf{X}_P])^2 - (\mathbb{E}[f_0(\mathbf{X}) \mid \mathbf{X}_P])^2] \right) - \left([\mathbb{E}f(\mathbf{X})]^2 - [\mathbb{E}f_0(\mathbf{X})]^2 \right) \right| \\ &\leq \mathbb{E} \left| (\mathbb{E}[f(\mathbf{X}) \mid \mathbf{X}_P])^2 - (\mathbb{E}[f_0(\mathbf{X}) \mid \mathbf{X}_P])^2 \right| + \left| [\mathbb{E}f(\mathbf{X})]^2 - [\mathbb{E}f_0(\mathbf{X})]^2 \right|. \end{aligned}$$

From the assumption that f and f_0 are bounded in supremum norm by C_0^* , we get

$$\begin{aligned} \left| [\mathbb{E}f(\mathbf{X})]^2 - [\mathbb{E}f_0(\mathbf{X})]^2 \right| &= \left| [\mathbb{E}f(\mathbf{X}) + \mathbb{E}f_0(\mathbf{X})][\mathbb{E}f(\mathbf{X}) - \mathbb{E}f_0(\mathbf{X})] \right| \\ &\leq 2C_0^* \mathbb{E}|f(\mathbf{X}) - f_0(\mathbf{X})|. \end{aligned}$$

We can similarly deduce for any \mathbf{X}_P that

$$\left| (\mathbb{E}[f(\mathbf{X}) \mid \mathbf{X}_P])^2 - (\mathbb{E}[f_0(\mathbf{X}) \mid \mathbf{X}_P])^2 \right| \leq 2C_0^* \mathbb{E}|f(\mathbf{X}) - f_0(\mathbf{X})| \mid \mathbf{X}_P].$$

Then

$$\begin{aligned} |c_{P,\pi}(f) - c_{P,\pi}(f_0)| &\leq \mathbb{E}[2C_0^* \mathbb{E}|f(\mathbf{X}) - f_0(\mathbf{X})| \mid \mathbf{X}_P] + 2C_0^* \mathbb{E}|f(\mathbf{X}) - f_0(\mathbf{X})| \\ &= 4C_0^* \mathbb{E}|f(\mathbf{X}) - f_0(\mathbf{X})|. \end{aligned}$$

To finish, Jensen's inequality implies $\mathbb{E}|f(\mathbf{X}) - f_0(\mathbf{X})| \leq \|f - f_0\|_{2,\pi}$. \square

Proof of Corollary 1. Below is the proof just for the j th (where $j \in [p]$) total-effect Sobol' index. The same argument can be followed to obtain the corresponding results for any main-effect Sobol' index and any Shapley effect after making the appropriate substitutions for the a_P below. Lemma 1 and Theorem 1 together imply

$$|T_{j,\pi}(f) - T_{j,\pi}(f_0)| \leq D_{T,\pi} \|f - f_0\|_{2,\pi}.$$

where $D_{T,\pi} \leq \max\{1, 4C_0^* \sum_{P \in [p]} |a_{P,\pi}|\}$ and the real values a_P are the coefficients corresponding to $T_{j,\pi}$ expressed as a linear combination of $c_{P,\pi}$. (Theorem 3 provides upper bounds for the sum $\sum_{P \in [p]} |a_{P,\pi}|$.) For any constant $\delta > 0$, define the two sets

$$\begin{aligned} A_\delta &:= \{(f, \sigma^2) : |T_{j,\pi}(f) - T_{j,\pi}(f_0)| + |\sigma^2 - \sigma_0^2| > \delta\} \\ B_\delta &:= \{(f, \sigma^2) : D_{T,\pi} |T_{j,\pi}(f) - T_{j,\pi}(f_0)| + D_{T,\pi} |\sigma^2 - \sigma_0^2| > \delta\}. \end{aligned}$$

Because $D_{T,\pi} \geq 1$, we have $A_\delta \subseteq B_\delta$ for all $\delta > 0$. Let $\mathcal{D}_n := \{(X_1, Y_1), \dots, (X_n, Y_n)\}$. By Theorem 4 of Jeong and Rockova (2023), there exists a constant $M > 0$ such that $\mathbb{E}_0 \Pi(B_{L_{T,\pi} \epsilon_n} \mid \mathcal{D}_n) \rightarrow 0$ as $n \rightarrow \infty$, where $L_{T,\pi} = D_{T,\pi} M$. Because $A_{L_{T,\pi} \epsilon_n} \subseteq B_{L_{T,\pi} \epsilon_n}$ for all n , we have $\mathbb{E}_0 \Pi(A_{L_{T,\pi} \epsilon_n} \mid \mathcal{D}_n) \rightarrow 0$ as $n \rightarrow \infty$. \square

The proofs of Theorem 2 and Corollary 2 can be obtained by replacing the random-design bound C_0^* with $\sqrt{\log n}$ and the distribution π with the probability measure $P_{\mathcal{X}}$.

Regarding the constant $D_{T,\pi}$ (and the corresponding constants $D_{V,\pi,|P|}$ and $D_{T,\pi}$) in the proof of Corollary 1, the sum $\sum_{P \in [p]} |a_{P,\pi}|$ seems to grow exponentially in p . Theorem 3 below states that this exponential dependence on p holds really only for a total-effect Sobol' index (although the sum for a Sobol' index V_P is $2^{|P|} - 1$, in practice such indices are computed only for $|P| \leq 3$). However, p is often much larger than the order of the

highest-order interaction in the true function. If the input distribution π is orthogonal (which is needed for a Sobol' index to be interpretable), if the true function does not contain interactions of order larger than $q \leq p$, and if the BART posterior assigns zero probability to functions with interactions of order larger than q (this third assumption is not unreasonable for even moderately large q , given that BART's prior discourages deep trees and a tree's regression function cannot have interactions of order larger than the tree's depth), then the sum's dependence on p for the total-effect index reduces to an exponential dependence on q , which is often quite small. (We can further reduce this dependence on q if π is orthogonal by omitting Sobol' index terms for subsets containing inert variables in a similar fashion as described in the proof of Theorem 3.)

Theorem 3. *Upper bounds for D_S , $D_{V,\pi,|P|}$, and $D_{T,\pi}$ in the proof of Corollary 1 are, respectively, $\max\{1, 8C_0^*\}$, $\max\{1, 4C_0^*(2^{|P|}-1)\}$, and $\max\{1, 4C_0^* \sum_{i=0}^{p-1} \binom{p-1}{i} (2^{i+1}-1)\}$. If π is orthogonal and neither f nor f_0 in Corollary 1 contain interactions of order larger than $q < p$, then the preceding upper bounds for $D_{V,\pi,|P|}$ and $D_{T,\pi}$ can be reduced to, respectively, $\max\{1, 4C_0^* \sum_{i=1}^{\min\{q,|P|\}} \binom{|P|}{i}\}$ and $\max\{1, 4C_0^* \sum_{i=0}^{q-1} \binom{q-1}{i} (2^{i+1}-1)\}$.*

Proof of Theorem 3. For the Shapley effect bound, we note that

$$\frac{1}{p} \sum_{P \subseteq ([p] \setminus \{j\})} \binom{p-1}{|P|}^{-1} = \frac{1}{p} \sum_{i=0}^{p-1} 1 = 1.$$

This with (8) and Theorem 1 together imply

$$\begin{aligned} |S_{j,\pi}(f) - S_{j,\pi}(f_0)| &\leq \left| \frac{1}{p} \sum_{P \subseteq ([p] \setminus \{j\})} \binom{p-1}{|P|}^{-1} [c_{P \cup \{j\},\pi}(f) - c_{P \cup \{j\},\pi}(f_0)] \right| \\ &\quad + \left| \frac{1}{p} \sum_{P \subseteq ([p] \setminus \{j\})} \binom{p-1}{|P|}^{-1} [c_{P,\pi}(f) - c_{P,\pi}(f_0)] \right| \\ &\leq 4C_0^* \|f - f_0\|_{2,\pi} + 4C_0^* \|f - f_0\|_{2,\pi}. \end{aligned}$$

As defined in Section 2.2, a Sobol' index $V_{P,\pi}(f)$ is a linear combination of costs (7) over all nonempty subsets of P , where each coefficient in the linear combination is either 1 or -1 . Since P has $\sum_{i=1}^{|P|} \binom{|P|}{i} = 2^{|P|} - 1$ many nonempty subsets, we can use Theorem 1 to get

$$|V_{P,\pi}(f) - V_{P,\pi}(f_0)| \leq (2^{|P|} - 1) 4C_0^* \|f - f_0\|_{2,\pi}.$$

If π is orthogonal and there are no interactions of order larger than q , then the Sobol' indices for the subsets of P containing more than q elements are zero, and hence we can omit those Sobol' indices from $V_{P,\pi}(f) - V_{P,\pi}(f_0)$. Since P has $\sum_{i=1}^{\min\{q,|P|\}} \binom{|P|}{i}$ many nonempty subsets containing at most q elements, the desired result follows.

As defined in Section 2.2, a total-effects Sobol' index $T_{j,\pi}(f)$ is the sum of $V_{P,\pi}(f)$ over

all subsets $P \subseteq [p]$ containing j . Using the above result, we get

$$\begin{aligned}
|T_{j,\pi}(f) - T_{j,\pi}(f_0)| &= \left| \sum_{P \subseteq ([p] \setminus \{j\})} V_{P \cup \{j\}, \pi}(f) - V_{P \cup \{j\}, \pi}(f_0) \right| \\
&\leq \sum_{P \subseteq ([p] \setminus \{j\})} (2^{|P|+1} - 1) 4C_0^* \|f - f_0\|_{2,\pi} \\
&\leq \sum_{i=0}^{p-1} \binom{p-1}{i} (2^{i+1} - 1) 4C_0^* \|f - f_0\|_{2,\pi}.
\end{aligned}$$

If π is orthogonal and there are no interactions of order larger than q , then the remaining result follows if we again omit from each sum the subsets of P containing more than q elements. \square